

Fluid-Glass-Jamming Rheology of Soft Active Brownian Particles

Roland Wiese,^{1,*} Klaus Kroy,¹ and Demian Levis^{2,3,†}

¹*Institute for Theoretical Physics, Leipzig University, 04103 Leipzig, Germany*

²*Departament de Física de la Materia Condensada, Facultat de Física, Universitat de Barcelona, Martí i Franquès 1, 08028 Barcelona, Spain*

³*University of Barcelona Institute of Complex Systems (UBICS), Facultat de Física, Universitat de Barcelona, Martí i Franquès 1, 08028 Barcelona, Spain*

(Dated: May 17, 2023)

We numerically study the shear rheology of a binary mixture of soft Active Brownian Particles, from the fluid to the disordered solid regime. At low shear rates, we find a Newtonian regime, where a Green-Kubo relation with an effective temperature provides the linear viscosity. It is followed by a shear-thinning regime at larger shear rates. At high densities, solidification is signalled by the emergence of a finite yield stress. We construct a “fluid-glass-jamming” phase diagram with activity replacing temperature. While both parameters gauge fluctuations, activity also changes the exponent characterizing the decay of the diffusivity close to the glass transition and the shape of the yield stress surface. The dense disordered active solid appears to be mostly dominated by athermal jamming rather than glass rheology.

Ensembles of repulsive particles commonly undergo a phase transition from a fluid to a solid state upon compression. If the tendency to crystallize is frustrated (e.g. by size polydispersity), thermal systems exhibit a glass transition to a disordered solid [1, 2]. Solidity can also emerge upon compression in athermal particle systems, such as foams or grains: the so-called jamming transition [3]. Both transitions share the existence of a critical density beyond which a yield stress emerges, heralded by a dramatic slowing down of the dynamics [4, 5]. Accordingly, a unified picture in terms of a “jamming” phase diagram was proposed [6, 7]. The yield stress surface has since been quantified with the help of idealized particle models and rheological experiments [8–11], helping to decipher and classify the mechanisms responsible for the emergence of rigidity in diverse soft materials [5].

A resurgence of interest in understanding the emergence of solidity is recently observed in an *a priori* completely new context, namely, dense disordered active matter. Indeed, assemblies of biological cells [12, 13] and synthetic active colloids [14] display a fluid to solid transition, key to understand tissue mechanics and morphogenesis. Moreover, they exhibit slow, collective dynamics, reminiscent of supercooled liquids approaching a glass transition. Again, this phenomenology has been rationalized in terms of a jamming phase diagram [15–18], where temperature is replaced by “activity”, usually in the form of motility, as in Fig. 1(a), where the Péclet number Pe quantifies the propulsion velocity of Active Brownian Particles (ABPs). While thermal fluctuations can usually be neglected in active systems, the effects of the (nonthermal) active fluctuations are often subsumed into an effective temperature. It is however conceptually unclear whether the emergence of a disordered solid should be attributed to a jamming or glass transition. The question of how self-propulsion affects a glass transition has already been addressed in numerous works using

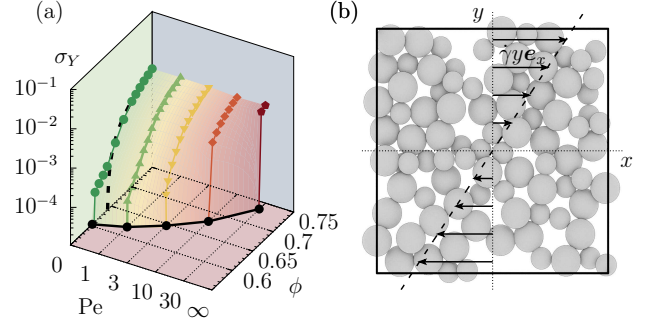


FIG. 1. Active “glass-jamming” rheology: (a) Yield stress surface of harmonic ABPs at reduced temperature $T = 10^{-4}$. The Péclet number Pe is a dimensionless measure of the active against the passive (thermal) particle motility and ϕ is the volume fraction. The dashed black line corresponds to the athermal ($T = 0$) passive jamming limit. The black symbols in the $Pe-\phi$ plane locate the active glass transition. (b) Cross section of the xy -plane of the three dimensional simulation box, showing the imposed velocity profile.

model systems [19–31]. Yet, despite considerable recent progress both for models of individual ABPs [32] and interacting active many-body systems [33–36], the rheology of dense active matter [37–39] and its relation with jamming, remains poorly understood. An analogy has been drawn between shear (a global drive) and activity (a local drive) [40], and indeed, in infinite spatial dimensions in the infinite-persistence limit, their formal equivalence has been established [41, 42]. In two dimensions, the mechanisms that govern yielding in the respective systems were found to be different, though [43]. Active particles under shear orientationally order in the presence of hard walls [35] and trigger shear thickening as a result of clustering [36]. However, the rheology of dense disordered ABPs with a finite persistence has not yet been explored.

In this Letter we investigate the shear rheology of self-

propelled soft particles by means of computer simulations. In previous experiments with microswimmer suspensions, both hydrodynamic and particle-wall interactions are likely to be crucial [44–48]. Here, in order to decipher the role played by self-propulsion alone, we consider a simplified model in which none of these two ingredients are at play [49]. More precisely, we consider a “dry” microswimmer model of harmonic ABPs in three dimensions [50, 51] with periodic boundary conditions (see Fig. 1(b)). The technical frugality allows us to cover the dilute and dense regimes in our numerical simulations, and to explore both linear and nonlinear response, across eight orders of magnitude in the shear rate. The advantages of choosing harmonic spheres are threefold: i) they have widely been employed as models for foams [52], and, if endowed with activity, provide a useful model for biological tissues [53, 54]; ii) the rheology of passive harmonic particles has been studied in detail [10, 11, 55], thus allowing for a smooth connection with previous results to discriminate the new features brought about by activity; iii) a computational speed-up compared to hard spheres.

In our simulations, N soft repulsive ABPs are placed at positions $\{\mathbf{r}_i\}_{i=1}^N$ in a $V = L^3$ cubic box with periodic boundary conditions. They self-propel along their orientations \mathbf{n}_i (with $|\mathbf{n}_i| = 1$), with a speed v_0 . Their otherwise overdamped Brownian dynamics obeys

$$\begin{aligned} \dot{\mathbf{r}}_i &= \mu \sum_{j \neq i} \mathbf{F}_{ij} + v_0 \mathbf{n}_i + \dot{\gamma} y_i \mathbf{e}_x + \sqrt{2D_t} \boldsymbol{\xi}_i, \\ \dot{\mathbf{n}}_i &= \sqrt{2D_r} \mathbf{n}_i \times \boldsymbol{\nu}_i. \end{aligned} \quad (1)$$

The interaction forces derive from a harmonic repulsive pair potential $V(r) = \epsilon (1 - r/a)^2 \Theta(a - r)$, $\Theta(r)$ being the Heaviside step function. To suppress crystallization we consider 50:50 bidisperse mixtures of $N = 10^3$ particles with diameters a and $\sqrt{2}a$, respectively [10, 56]. Both $\boldsymbol{\xi}_i$ and $\boldsymbol{\nu}_i$ are Gaussian white noises of zero mean and unit variance, $D_t = \mu k_B T$ is the (bare) translational diffusion coefficient, and D_r the rotational diffusivity fixed to $D_r = 3D_t/a^2$. With this choice, $T \rightarrow 0$ corresponds to infinite persistence. To further explore the athermal case we fix $D_t = 0$ and vary D_r independently. We impose a linear velocity profile on the particles and apply Lees-Edwards boundary conditions (see Fig. 1(b)) [57, 58]. The translational part of Eq.(1) is integrated by an Euler-Mayurama scheme and the rotational part using the algorithm described in [59] (see [60] for details).

Lengths are measured in units of the small particle diameter a , time t in units of $a^2/(\mu\epsilon)$ and temperature T in units of ϵ/k_B . In the following, all observables will be given in these units. From Eq.(1), one can identify a set of nondimensional control parameters: the volume fraction ϕ , the Péclet number $Pe = v_0/aD_r$, quantifying activity, and the dimensionless shear rate $\dot{\gamma}$. We study the system at $T = 10^{-6} \dots 10^3$ (most of the results presented

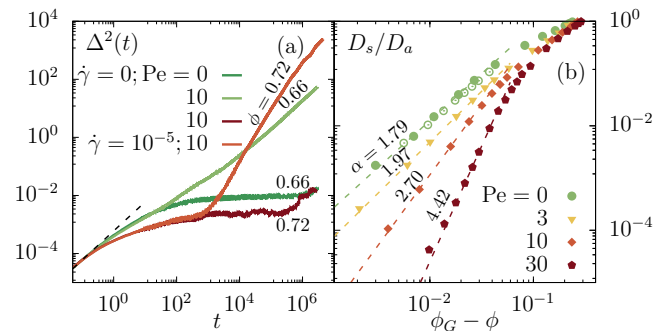


FIG. 2. Dynamic signatures of melting: (a) mean-square displacement at fixed $T = 10^{-4}$, $Pe = 0$ and 10 , for $\phi = 0.66, 0.72$, with and without shear, showing the melting of the glass by activity (green curves) and by shear (red curves). The dashed line indicates the initial diffusive regime, $\Delta^2(t) = 6D_t t$. (b) Diffusion coefficients D_s normalized by their ideal gas value D_a (open green circles correspond to $T = 10^{-3}$ and $Pe = 0$), as a function of the distance to the critical density $\phi_G - \phi$. Dashed lines are power law fits $D_s \propto (\phi_G - \phi)^\alpha$.

are for $T = 10^{-4}$), $Pe = 0, 1, 3, 10, 30$, and a wide range of shear rates $\dot{\gamma} = 10^{-7} \dots 10$, including both the linear and nonlinear response regimes. With this choice of parameters and constant D_r , the system remains homogeneous and avoids Motility-Induced Phase Separation, which is known to occur for monodisperse hard ABPs above a critical $Pe \approx 30$ [50, 51, 61]. Also, the repulsive force is always several orders of magnitude larger than the self-propulsion to avoid a reentrant gas phase, as seen in [62].

In equilibrium ($Pe = 0$), as ϕ is increased, the system exhibits a dramatic slowing down of the dynamics that one identifies with a glass transition at ϕ_G , characterized by the divergence of the viscosity and the emergence of a yield stress for $\phi > \phi_G(0)$. As we show below, similar behavior is observed in the presence of activity, although in this case, the location of the glass transition is shifted to higher densities $\phi_G(Pe)$, as previously reported for diverse models [20–23, 30, 63, 64].

We start our analysis by investigating the dynamics in the absence of shear by means of the Mean-Square Displacement (MSD), defined as $\Delta^2(t) = N^{-1} \sum_{i=1}^N \langle (\mathbf{r}_i(t) - \mathbf{r}_i(0))^2 \rangle$, where the average is taken over different noise realisations. As shown in Fig. 2(a), at $\phi = 0.66$ the passive system exhibits caged dynamics, evidenced by the sub-diffusive (plateau) regime. For $Pe = 10$, particles diffuse in the same time window, showing that activity is able to fluidize the glass. At long times we extract the diffusion coefficient $D_s \equiv \lim_{t \rightarrow \infty} \Delta^2(t)/6t$ in the range of parameters for which a diffusive regime, $\Delta^2(t) \propto t$, is observed. At high densities, $D_s(\phi)$ can be fitted by a power law $D_s \propto (\phi_G - \phi)^\alpha$ that we use to locate the glass transition density reported in Fig. 1(a) [21]. Figure 2(b) shows $D_s(\phi, Pe)$ as a function of $(\phi_G - \phi)$ normalized by the (active) ideal gas diffusion coefficient

$D_a = D_t + \text{Pe}^2 D_r / 6$, for different Pe. As the activity primarily enhances diffusion, it moves the glass transition from $\phi_G(0) = 0.62$ at Pe = 0 to ever higher densities, up to $\phi_G(30) = 0.72$ at Pe = 30 (see Fig. 1(a)). It might be tempting to simply interpret such a shift as resulting from an increase of the single particle effective temperature, defined by $T_{\text{eff}} = \mu D_a$, since the equilibrium glass transition density would also be shifted upon increasing T [65]. However, not only ϕ_G is affected by activity, but also the exponent α increases from 1.79 at Pe = 0, up to 4.42 at Pe = 30. While in equilibrium a slightly lower value ($\alpha = 1.67$) is measured for higher temperature $T = 10^{-3}$, α significantly changes with Pe, showing that activity cannot simply be reduced to an effective temperature in this regime.

Applying shear provides another route to fluidize the disordered solid state. As shown in Fig. 2(a), particles exhibiting caged dynamics in an active system at $\phi = 0.72 > \phi_G(10)$, become mobile upon shearing. The MSD displays super-diffusive, then diffusive behavior at long times. The obtained long time diffusion is sensitive to finite-size effects: Lees-Edwards boundary conditions introduce a discontinuity in the shear profile which becomes apparent in the MSD after a sufficiently long time (see [60] for details).

To characterize the flow properties we measure the xy -component of the stress tensor, using the Irving-Kirkwood expression [66] $\sigma_{xy}(t) = -(2V)^{-1} \sum_{j \neq k} x_{ij}(t) F_{ij}^y(t)$, from which we get the shear viscosity $\eta = \langle \sigma_{xy} \rangle / \dot{\gamma}$. Activity contributes to the stress tensor with a self-term $\sigma_{\alpha\beta}^s = -V^{-1} \sum_i r_i^\alpha v_i n_i^\beta(t)$, but as the orientations \mathbf{n}_i are decoupled from the shear flow, σ_{xy}^s fluctuates around zero [35]. The flow curves characterizing the rheology of the system at $T = 10^{-4}$ and Pe = 0, 10 are depicted in Fig. 3 (see [60] for more parameter values). In the passive case, Pe = 0, we reproduce the flow curves reported for the same system in [10]. Then, we explore the rheology in the presence of activity. In dense two-dimensional active assemblies, shearing was observed to lead to orientational order at large persistence time [35]. However, we did not find orientational correlations in our three-dimensional model for the parameter range explored (see [60]).

At densities below $\phi_G(\text{Pe})$, we find $\sigma_{xy} \propto \dot{\gamma}$ for small enough applied shear. This corresponds to the Newtonian fluid regime, defining a linear viscosity $\eta_0 = \lim_{\dot{\gamma} \rightarrow 0} \langle \sigma_{xy} \rangle / \dot{\gamma}$. For higher values, $\dot{\gamma} \gtrsim 10^{-2}$, in the non-linear regime, we find shear-thinning in all cases, meaning that the shear flow reduces the system's viscosity. In this regime, we find a decay of the viscosity compatible with the $\eta \sim 1/|\dot{\gamma}|$ scaling expected from Mode-Coupling Theory for Brownian suspensions [67]. At $\phi > \phi_G$, a finite yield stress $\sigma_Y = \lim_{\dot{\gamma} \rightarrow 0} \sigma_{xy}(\dot{\gamma})$ appears, identified by a plateau in the stress flow curves. This results in a divergent viscosity, signalling the emergence of solidity. Since activity melts the solid, the system yields at higher

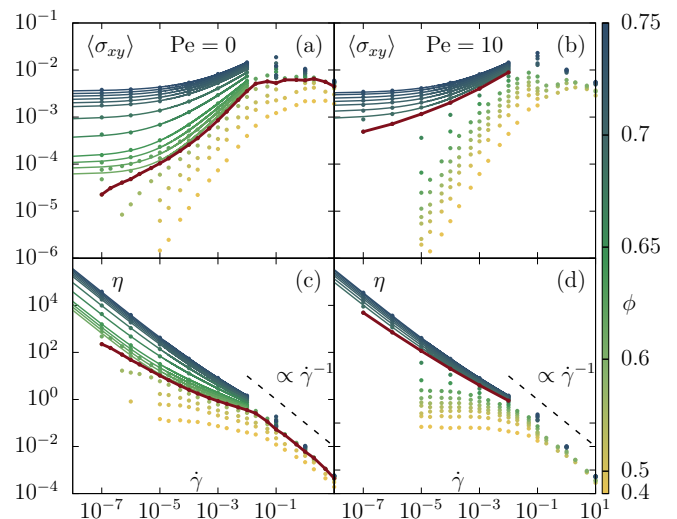


FIG. 3. Flow curves for shear stress $\langle \sigma_{xy} \rangle(\dot{\gamma})$ (top) and viscosity $\eta(\dot{\gamma})$ (bottom). Color encodes ϕ , the thick red lines correspond to ϕ_G (as estimated via the diffusivity) and thin lines represent fits of the form $\sigma_{xy}(\dot{\gamma}) = \sigma_Y + (k\dot{\gamma})^n$, used to determine the yield stress σ_Y .

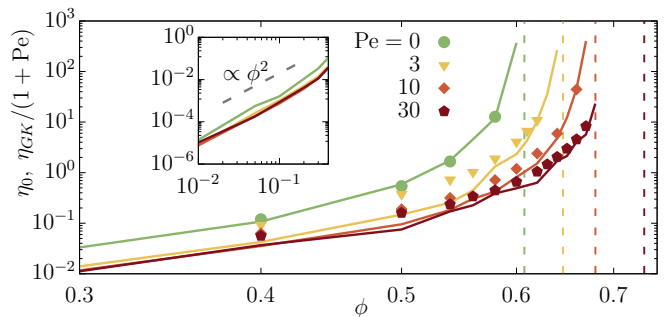


FIG. 4. Density-dependent linear shear viscosity η_0 , extracted from the flow curves (symbols), and $\eta_{GK}/(\text{Pe} + 1)$, from Green-Kubo, (lines). Dashed vertical lines indicate $\phi_G(\text{Pe})$. Inset: $\eta_{GK} \propto \phi^2$ at low densities.

densities at Pe = 10 compared to Pe = 0.

In the fluid regime, one can access the linear viscosity by applying small enough shear and, in equilibrium, it should correspond to the one given by the Green-Kubo (GK) relation $\eta_{GK} = \frac{V}{k_B T} \int_0^\infty dt \langle \sigma_{\alpha\beta}(t) \sigma_{\alpha\beta}(0) \rangle_0$, for $\alpha \neq \beta$, where $\langle * \rangle_0$ denotes an average over the unperturbed ($\dot{\gamma} = 0$) equilibrium distribution. As shown in Fig. 4, the shear viscosity η_0 extracted from the low $\dot{\gamma}$ plateau in the flow curves in Fig. 3(c) matches η_{GK} , measured from the GK relation by direct integration of the equilibrium stress correlation function. In the presence of activity, GK relations do not need to hold anymore, although extensions of linear response theory to active systems have recently been proposed [68–71], providing GK relations involving steady-state correlation functions [68, 70]. Here we apply the same procedure in the pres-

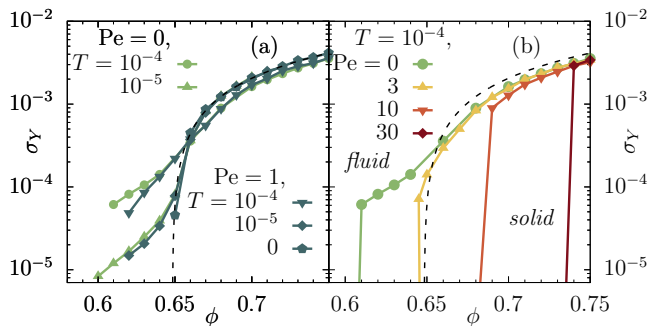


FIG. 5. Yield stress σ_Y as a function of ϕ for different Pe and T . The dashed line given by $(\phi - \phi_J)^{\alpha'}$ with $\phi_J = 0.648$ and $\alpha' = 1.04$, marks the athermal jamming limit.

ence of activity, thus replacing equilibrium by steady-state stress correlations, and find a good agreement between η_0 and η_{GK} if we replace T in the GK expression by an effective temperature $T_{\text{eff}} = T(Pe + 1)$, see Fig. 4. In all cases, η_0 increases with ϕ and eventually diverges at ϕ_G , providing yet another estimate for the onset of solidity. In dilute conditions, we find that the GK viscosity grows like $\sim \phi^2$ (inset of Fig. 4), as predicted for dilute Brownian suspensions: $\eta/\eta_0 = 1 + 2.5\phi + 7.6\phi^2$ [72]. We only observe the ϕ^2 contributions, as there is no solvent in our system.

Above ϕ_G the viscosity diverges and the system acquires a yield stress σ_Y that we measure by fitting a Herschel-Bulkley law, $\sigma_{xy}(\dot{\gamma}) = \sigma_Y + (k\dot{\gamma})^n$ [73], to the flow curves, see Fig. 3. We report the obtained yield stress $\sigma_Y(\phi)$ as a function of volume fraction for different values of Pe and T in Fig. 5. At $Pe = 0$ and finite T , the emergence of solidity is controlled by the glass transition, at a critical density $\phi_G(T)$ that increases with T . At $T = 0$, it is instead controlled by the jamming transition, at $\phi_J \approx 0.648$. Both glass and jamming physics affect the shape of the yield surface of $\sigma_Y(\phi, T)$. At $T \leq 10^{-4}$, for which $\phi_G < \phi_J$, σ_Y increases gently with ϕ and T up to $\phi \approx \phi_J$ (indicated by dashed lines in Fig. 5). Above this value, the behavior of σ_Y changes qualitatively: it grows faster with ϕ close to ϕ_J , with little T -dependence, following $\sigma_Y \sim (\phi - \phi_J)^{\alpha'}$ [10], see Fig. 5(a). Such crossover allows us to differentiate glass- and jamming-dominated regimes.

At $Pe = 1$ and finite T , σ_Y displays a T -sensitive glass-like branch for $\phi < \phi_J$ followed by the T -insensitive jamming branch, see Fig. 5(a). The yield stress curves do not follow the trend one would expect if activity could be subsumed into an extra source of noise and encoded by an increased effective temperature. The yield stress is smaller for $Pe = 1$ than for $Pe = 0$, at a given ϕ and T , up to ϕ_J . A higher T would instead result in a larger σ_Y . Moreover, at $T = 0$, we recover again the athermal jamming behavior, despite the presence of random (active) forces. As we further increase the activity at fixed

$T = 10^{-4}$, σ_Y quickly collapses onto the jamming branch. For $Pe > 3$, $\phi_G(Pe) > \phi_J$, and a finite yield stress can only emerge in the parameter regime controlled by jamming [56], where $\sigma_Y \sim (\phi - \phi_J)^{\alpha'}$ universally applies, independently of Pe . The crossover between glass and jamming rheology can thus be tuned by activity and is eventually lost, as it pushes σ_Y towards the athermal limit. The separation between ϕ_G and ϕ_J progressively vanishes as activity increases. An overview over the impact of activity on the yield surface at $T = 10^{-4}$ is represented in the fluid-glass-jamming phase diagram in Fig. 1.

We have studied ABPs under shear, from its fluid to disordered solid regime. In the fluid, taking the zero shear limit, the Green-Kubo viscosities are compatible with the ones extracted from the flow curves in the Newtonian regime, once the Brownian temperature T is replaced by an effective temperature that depends on the active Péclet number. This strategy follows earlier ideas to quantify the violations of the fluctuation-dissipation theorem in active systems. In the dilute limit, $T_{\text{eff}} \sim Pe^2$. At intermediate densities T_{eff} generically depends on the observables used to define it [22, 68, 74]. As the packing fraction is increased towards the fluid-solid transition, the diffusivity decays $D_s \sim (\phi_G - \phi)^\alpha$, with α increasing from $\alpha \approx 1.8$ for $Pe = 0$, to $\alpha \approx 4.4$ for $Pe = 30$, a behavior hardly interpretable on the grounds of an effective temperature anymore. The glass-jamming phase diagram (Fig. 1) reveals that ABP rheology in the solid regime is mainly controlled by jamming. Although both T and Pe push ϕ_G to higher values, activity, as opposed to temperature, eases the yielding, and, in this respect, could rather play a role similar to shear, as our particles' persistence length exceeds the typical cage length [41]. Our work thus calls for further theoretical efforts to better understand the fundamental role played by non-equilibrium fluctuations introduced by activity in dense disordered systems, for instance, extending elastoplastic models of yielding to account for self-propulsion or analyzing dynamic heterogeneities in active glasses [75–78]. Providing the first quantitative jamming phase diagram of an active system, our work should serve as a helpful reference for future studies, helping to interpret observations in dense assemblies of cells, for which only qualitative phase diagrams have been sketched [15–18], and eventually shedding light on the relationship between the glass and jamming transitions in biological systems.

Acknowledgments We warmly thank T. Voigtmann, I. Pagonabarraga, S. Dal Cengio, A. Ikeda and L. Berthier for useful exchanges. D.L. acknowledges MCIU/AEI/FEDER for financial support under Grant Agreement No. RTI2018-099032-J-I00.

* wiese@itp.uni-leipzig.de

† levis@ub.edu

- [1] P. N. Pusey and W. van Meegen, *Nature* **320**, 340–342 (1986).
- [2] J. Mewis and N. J. Wagner, *Colloidal suspension rheology* (Cambridge University Press, 2011).
- [3] A. J. Liu and S. R. Nagel, *Annu. Rev. Condens. Matter Phys.* **1**, 347–369 (2010).
- [4] L. Berthier and G. Biroli, *Rev. Mod. Phys.* **83**, 587 (2011).
- [5] D. Bonn, M. M. Denn, L. Berthier, T. Divoux, and S. Manneville, *Rev. Mod. Phys.* **89**, 035005 (2017).
- [6] A. J. Liu and S. R. Nagel, *Nature* **396**, 21–22 (1998).
- [7] V. Trappe, V. Prasad, L. Cipelletti, P. N. Segre, and D. A. Weitz, *Nature* **411**, 772–775 (2001).
- [8] M. P. Ciamarra, M. Nicodemi, and A. Coniglio, *Soft Matter* **6**, 2871 (2010).
- [9] T. K. Haxton, M. Schmiedeberg, and A. J. Liu, *Phys. Rev. E* **83**, 031503 (2011).
- [10] A. Ikeda, L. Berthier, and P. Sollich, *Phys. Rev. Lett.* **109**, 018301 (2012).
- [11] A. Ikeda, L. Berthier, and P. Sollich, *Soft Matter* **9**, 7669 (2013).
- [12] T. E. Angelini, E. Hannezo, X. Trepate, M. Marquez, J. J. Fredberg, and D. A. Weitz, *Proc. Natl. Acad. Sci.* **108**, 4714–4719 (2011).
- [13] E.-M. Schötz, M. Lanio, J. A. Talbot, and M. L. Manning, *J. R. Soc. Interface* **10**, 20130726 (2013).
- [14] N. Klongvessa, F. Ginot, C. Ybert, C. Cottin-Bizonne, and M. Leocmach, *Phys. Rev. Lett.* **123**, 248004 (2019).
- [15] A. Mongera, P. Rowghanian, H. J. Gustafson, E. Shelton, D. A. Kealhofer, E. K. Carn, F. Serwane, A. A. Lucio, J. Giammona, and O. Campàs, *Nature* **561**, 401–405 (2018).
- [16] E. Lawson-Keister and M. L. Manning, *Curr. Opin. Cell Biol.* **72**, 146–155 (2021).
- [17] P.-F. Lenne and V. Trivedi, *Nat. Commun.* **13** (2022).
- [18] S. Kim, R. Amini, and O. Campàs 10.1101/2022.07.31.502244 (2022).
- [19] L. Berthier and J. Kurchan, *Nature Phys.* **9**, 310 (2013).
- [20] R. Ni, M. A. C. Stuart, and M. Dijkstra, *Nat. Commun.* **4** (2013).
- [21] L. Berthier, *Phys. Rev. Lett.* **112** (2014).
- [22] D. Levis and L. Berthier, *Europhys. Lett.* **111**, 60006 (2015).
- [23] L. Berthier, E. Flenner, and G. Szamel, *New J. Phys.* **19**, 125006 (2017).
- [24] D. Bi, X. Yang, M. C. Marchetti, and M. L. Manning, *Phys. Rev. X* **6** (2016).
- [25] D. M. Sussman, M. Paoluzzi, M. Cristina Marchetti, and M. Lisa Manning, *Europhys. Lett.* **121**, 36001 (2018).
- [26] L. M. C. Janssen, *J. Phys. Condens. Matter* **31**, 503002 (2019).
- [27] M. Czajkowski, D. M. Sussman, M. C. Marchetti, and M. L. Manning, *Soft Matter* **15**, 9133–9149 (2019).
- [28] S. Henkes, K. Kostanjevec, J. M. Collinson, R. Sknepnek, and E. Bertin, *Nat. Comm.* **11**, 1405 (2020).
- [29] S. Sadhukhan and S. K. Nandi, *Phys. Rev. E* **103** (2021).
- [30] M. Paoluzzi, D. Levis, and I. Pagonabarraga, *Commun. Phys.* **5**, 1 (2022).
- [31] Y.-E. Keta, R. L. Jack, and L. Berthier, *Phys. Rev. Lett.* **129**, 048002 (2022).
- [32] B. ten Hagen, R. Wittkowski, and H. Löwen, *Phys. Rev. E* **84** (2011).
- [33] K. Asheichyk, A. P. Solon, C. M. Rohwer, and M. Krüger, *J. Chem. Phys.* **150**, 144111 (2019).
- [34] J. Reichert, L. F. Granz, and T. Voigtmann, *Eur. Phys. J. E* **44**, 1 (2021).
- [35] R. Mandal and P. Sollich, *Proc. Natl. Acad. Sci.* **118** (2021).
- [36] A. G. Bayram, F. J. Schwarzendahl, H. Löwen, and L. Biancofiore, [arXiv:2301.05429 \[cond-mat.soft\]](https://arxiv.org/abs/2301.05429) (2023).
- [37] A. Peshkov, P. Claudin, E. Clément, and B. Andreotti, *Europhys. Lett.* **116**, 14001 (2016).
- [38] D. A. Matoz-Fernandez, K. Martens, R. Sknepnek, J. L. Barrat, and S. Henkes, *Soft Matter* **13**, 3205–3212 (2017).
- [39] A. Amiri, C. Duclut, F. Jülicher, and M. Popović, [arXiv:2211.02159v1 \[cond-mat.soft\]](https://arxiv.org/abs/2211.02159v1) (2022).
- [40] R. Mo, Q. Liao, and N. Xu, *Soft Matter* **16**, 3642–3648 (2020).
- [41] P. K. Morse, S. Roy, E. Agoritsas, E. Stanifer, E. I. Corwin, and M. L. Manning, *Proc. Natl. Acad. Sci.* **118**, e2019909118 (2021).
- [42] E. Agoritsas, *J. Stat. Mech.* **2021**, 033501 (2021).
- [43] C. Villarroel and G. Düring, *Soft Matter* **17**, 9944–9949 (2021).
- [44] S. Rafai, L. Jibuti, and P. Peyla, *Phys. Rev. Lett.* **104**, 098102 (2010).
- [45] J. Gachelin, G. Miño, H. Berthet, A. Lindner, A. Rousselet, and E. Clément, *Phys. Rev. Lett.* **110**, 268103 (2013).
- [46] H. M. López, J. Gachelin, C. Douarche, H. Auradou, and E. Clément, *Phys. Rev. Lett.* **115**, 028301 (2015).
- [47] D. Saintillan, *Annu. Rev. of Fluid Mech.* **50**, 563 (2018).
- [48] V. A. Martinez, E. Clément, J. Arlt, C. Douarche, A. Dawson, J. Schwarz-Linek, A. K. Creppy, V. Škultéty, A. N. Morozov, H. Auradou, and W. C. K. Poon, *Proc. Natl. Acad. Sci.* **117**, 2326–2331 (2020).
- [49] M. R. Shaebani, A. Wysocki, R. G. Winkler, G. Gompper, and H. Rieger, *Nature Rev. Phys.* **2**, 181 (2020).
- [50] A. Wysocki, R. G. Winkler, and G. Gompper, *Europhys. Lett.* **105**, 48004 (2014).
- [51] F. Turci and N. B. Wilding, *Phys. Rev. Lett.* **126** (2021).
- [52] D. J. Durian, *Phys. Rev. Lett.* **75**, 4780–4783 (1995).
- [53] D. A. Matoz-Fernandez, E. Agoritsas, J.-L. Barrat, E. Bertin, and K. Martens, *Phys. Rev. Lett.* **118** (2017).
- [54] A. N. Malmi-Kakkada, X. Li, H. S. Samanta, S. Sinha, and D. Thirumalai, *Phys. Rev. X* **8**, 021025 (2018).
- [55] M. Trulsson, M. Bouzid, J. Kurchan, E. Clément, P. Claudin, and B. Andreotti, *Europhys. Lett.* **111**, 18001 (2015).
- [56] P. Olsson and S. Teitel, *Phys. Rev. Lett.* **99**, 178001 (2007).
- [57] A. W. Lees and S. F. Edwards, *J. Phys. C* **5**, 1921–1928 (1972).
- [58] M. P. Allen and D. J. Tildesley, *Computer Simulation of Liquids* (Oxford University Press, 2017).
- [59] M. Raible and A. Engel, *Appl. Organometal. Chem.* **18**, 536–541 (2004).
- [60] See supplemental material at *URL will be inserted by publisher* for more details on the algorithm, phase separation, further rheological results. (2023).
- [61] A. K. Omar, K. Klymko, T. GrandPre, and P. L. Geissler, *Phys. Rev. Lett.* **126** (2021).
- [62] Y. Fily, S. Henkes, and M. C. Marchetti, *Soft Matter* **10**, 2132 (2014).
- [63] L. Berthier and J. Kurchan, *Nat. Phys.* **9**, 310 (2013).

- [64] S. Henkes, Y. Fily, and M. C. Marchetti, *Phys. Rev. E* **84** (2011).
- [65] L. Berthier and T. A. Witten, *Phys. Rev. E* **80**, 021502 (2009).
- [66] J. H. Irving and J. G. Kirkwood, *J. Chem. Phys.* **18**, 817–829 (1950).
- [67] M. Fuchs and M. E. Cates, *J. Phys. Condens. Matter* **15**, S401–S406 (2002).
- [68] S. Dal Cengio, D. Levis, and I. Pagonabarraga, *Phys. Rev. Lett.* **123**, 238003 (2019).
- [69] K. Asheichyk, A. P. Solon, C. M. Rohwer, and M. Krüger, *J. Chem. Phys.* **150**, 144111 (2019).
- [70] S. Dal Cengio, D. Levis, and I. Pagonabarraga, *J. Stat. Mech.* **2021**, 043201 (2021).
- [71] L. P. Dadhichi and K. Kroy, *Phys. Rev. E* **107** (2023).
- [72] G. K. Batchelor and J. T. Green, *J. Fluid Mech.* **56**, 401 (1972).
- [73] W. H. Herschel and R. Bulkley, *Kolloid Z.* **39**, 291–300 (1926).
- [74] I. Petrelli, L. F. Cugliandolo, G. Gonnella, and A. Suma, *Phys. Rev. E* **102**, 012609 (2020).
- [75] R. Yamamoto and A. Onuki, *Phys. Rev. E* **58**, 3515–3529 (1998).
- [76] T. Voigtmann, *Curr. Opin. Colloid Interface Sci.* **19**, 549–560 (2014).
- [77] A. Nicolas, E. E. Ferrero, K. Martens, and J.-L. Barrat, *Rev. Mod. Phys.* **90** (2018).
- [78] K. Kamani, G. J. Donley, and S. A. Rogers, *Phys. Rev. Lett.* **126** (2021).